HHS Public Access

Author manuscript

Circulation. Author manuscript; available in PMC 2017 August 30.

Published in final edited form as:

Circulation. 2016 August 30; 134(9): 666–680. doi:10.1161/CIRCULATIONAHA.116.021894.

Resolvin D2 Enhances Post-Ischemic Revascularization While Resolving Inflammation

Michael J. Zhang, Ph.D.[#2], **Brian E. Sansbury, Ph.D.**[#1], **Jason Hellmann, Ph.D.**[1], **James F. Baker**[2], **Luping Guo, M.D.**[2], **Caitlin M. Parmer**[3], **Joshua C. Prenner**[3], **Daniel J. Conklin, Ph.D.**[2], **Aruni Bhatnagar, Ph.D.**[2], **Mark A. Creager, M.D.**[3], and **Matthew Spite, Ph.D.**[1]

[1]Center for Experimental Therapeutics and Reperfusion Injury, Department of Anesthesiology, Perioperative and Pain Medicine, Brigham and Women's Hospital and Harvard Medical School, Harvard Institutes of Medicine, Boston, MA

[2]Institute of Molecular Cardiology, Diabetes and Obesity Center, Division of Cardiovascular Medicine, University of Louisville School of Medicine, Louisville, KY

[3]Vascular Medicine Section, Cardiovascular Division, Brigham and Women's Hospital and Harvard Medical School, Boston, MA

[#] These authors contributed equally to this work.

Abstract

Background—Resolvins are lipid mediators generated by leukocytes during the resolution phase of inflammation. They have been shown to regulate the transition from inflammation to tissue repair; however, it is unknown whether resolvins play a role in tissue revascularization following ischemia.

Methods—We used a murine model of hind limb ischemia (HLI), coupled with laser Doppler perfusion imaging, micro computed tomography (microCT) and targeted mass spectrometry, to assess the role of resolvins in revascularization and inflammation-resolution.

Results—In mice undergoing HLI, we identified resolvin D2 (RvD2) in bone marrow and skeletal muscle by mass spectrometry (n=4-7 per group). We also identified RvD2 in skeletal muscle biopsies from humans with peripheral artery disease. Monocytes were recruited to skeletal muscle during HLI and isolated monocytes produced RvD2 in a lipoxygenase-dependent manner. Exogenous RvD2 enhanced perfusion recovery in HLI and microCT of limb vasculature revealed greater volume, with evidence of tortuous arterioles indicative of arteriogenesis (n=6-8 per group). Unlike other treatment strategies for therapeutic revascularization that exacerbate inflammation, RvD2 did not increase vascular permeability, but reduced neutrophil accumulation and the plasma levels of TNF-α and GM-CSF. In mice treated with RvD2, histopathological analysis of skeletal muscle of ischemic limbs showed more regenerating myocytes with centrally located nuclei. RvD2 enhanced endothelial cell migration in a Rac-dependent manner, via its receptor, GPR18, and

Correspondence to Matthew Spite, Ph.D., Harvard Institutes of Medicine, 77 Avenue Louis Pasteur, HIM830, Boston, MA 02115, Ph: 617-525-5133, mspite@bwh.harvard.edu.
Present address for Mark A. Creager: Dartmouth-Hitchcock Heart and Vascular Center, Dartmouth College, Hanover, NH

Disclosures
None

Gpr18-deficient mice had an endogenous defect in perfusion recovery following HLI. Importantly, RvD2 rescued defective revascularization in diabetic mice.

Conclusions—RvD2 stimulates arteriogenic revascularization during HLI suggesting that resolvins may be a novel class of mediators that both resolve inflammation and promote arteriogenesis.

Keywords

peripheral vascular disease; revascularization; inflammation; imaging

Arterial occlusion during peripheral artery disease (PAD) impairs tissue perfusion and in its most advanced stage, can lead to critical limb ischemia (CLI) and limb loss[1-3]. Arteriogenesis (i.e., collateral vessel growth) is an endogenous process that partially compensates for defects in tissue perfusion[4]. Arteriogenesis is stimulated by increased shear stress associated with diversion of blood flow proximal to the occlusion into pre-existing collateral arteriolar connections, as well as by growth factors and cytokines[5, 6]. Although arteriogenesis partially compensates for reduced blood flow after occlusion, the endogenous process could be enhanced therapeutically[5, 7].

Arteriogenesis is tightly coupled to the inflammatory response; monocytes and macrophages recruited to the tissue secrete growth factors that promote endothelial cell migration and proliferation, as well as mural cell recruitment and differentiation[6]. Monocytes are sufficient to enhance revascularization in mouse models of HLI and mice deficient in monocyte chemotaxis (e.g., *Ccr2*) have impaired perfusion recovery[6, 8-10]. Several therapeutic strategies have been tested to increase arteriogenesis, including growth factors and mononuclear cells. However, the efficacy of these approaches has met limited success in large clinical trials, which could be related to the chronic inflammatory environment typically encountered in patients with PAD[7]. Importantly, most factors that promote revascularization are also pro-inflammatory and can increase atherosclerosis, potentially limiting their therapeutic use in patients with PAD[7, 11, 12].

Recent studies indicate that resolution of inflammation is important for the transition to tissue repair during wound healing[13]. Resolution is an active process that involves the generation of pro-resolving lipid mediators, such as the resolvins[14]. Resolvins have receptor-dependent anti-inflammatory actions that include decreasing neutrophil trafficking to inflammatory loci and attenuating pro-inflammatory cytokine production[14, 15]. They also stimulate macrophage-mediated clearance of apoptotic cells and promote tissue repair and regeneration[13]. Resolvins regulate leukocyte-endothelial interactions and have direct receptor-mediated signaling roles in endothelial cells[16-18]. Hence, we asked whether resolvins play a role in revascularization.

Methods

Animals and reagents

Male C57BL/6J (WT) mice, leptin receptor-deficient (*db/db*) mice, and 12/15-lipoxygenase (LOX)-deficient mice (*Alox15*^{tm1fun}) on a C57BL/6J background were purchased from

Jackson Laboratories (Bar Harbor, ME) at 8-10 weeks of age. *Gpr18*-deficient mice and their WT littermates are on a mixed 129/SvEv-C57B/6 background. Resolvin D2 (RvD2; 7*S*,16*R*,17*S*-trihydroxy-4*Z*,8*E*,10*Z*,12*E*,14*E*,19*Z*-docosahexaenoic acid) was purchased from Cayman Chemical (Ann Arbor, MI). All animal procedures were approved by the Harvard Medical Area Standing Committee on animals or the University of Louisville IACUC.

Surgical hind limb ischemia model

For the surgical induction of hind limb ischemia (HLI)[19], mice were anesthetized with 2% isoflurane (with 2 L/min O_2) and maintained on a temperature controlled water blanket at 37°C. Depilatory cream was applied to the limbs and the area was sterilized by 70% ethanol applications. A 5-mm vertical skin incision was made lateral to the abdomen and superficial to the inguinal ligament. The inguinal fat pad was separated from the peritoneal lining to reveal the proximal femoral artery branching from the internal iliac artery. The femoral artery and vein were then separated from the membrane sheath and two ligatures were tied around both vessels approximately 2-mm apart[20-22]. Vessels were transected between the ligatures and the skin incision was closed with two discontinuous sutures and bonded with *n*-butyl-ester cyanoacrylate. Sham operated mice were opened, dissected, and closed without vessel ligature. In some cases, a less-severe model of HLI was used. For this, a 3mm horizontal skin incision was made superficial to the medial right knee. The branch point where the femoral artery bifurcates into the saphenous artery and popliteal artery was exposed from its membrane sheath. The accompanying nerve was carefully avoided and a ligature was placed around the saphenous artery and vein immediately distal to the femoral bifurcation. A second ligature was tied approximately 1mm below the first, and vessels were then transected between ligatures. The skin was then closed with sutures and cyanoacrylate. Buprenorphine (0.5mg/kg) was given twice within 24h post-surgery. Twenty-four hours after surgery, mice were injected with either 0.9% saline vehicle (100 μl), or RvD2 in vehicle (1ng/μl; 100 μl) subcutaneously and just superficial to the ligation site. Treatments were given daily until euthanasia.

Perfusion imaging

Limb perfusion was assessed by laser Doppler perfusion imaging (LDPI). For this, mice were anesthetized with isoflurane and placed on a dark scanning surface. Perfusion of the ventral surface of both right and left hind limbs was measured with a PeriScan PIM 2 laser Doppler device (Perimed). Images were acquired one, seven and fourteen days after ligation. After acquisition, color-binned images of the mouse limbs were imported into ImageJ, and areas of blue, green and red in the region of interest (ROI) spanning the entire hind limb were enumerated. The value for the right ischemic limb was then normalized to the left (non-ischemic) limb to calculate the % recovery of blood perfusion for each mouse. For experiments with *Gpr18*-deficient mice and *db/db* mice, limb perfusion was measured by infrared laser speckle contrast analysis using a moorFLPI-2 full-field laser perfusion imager (Moor Instruments). Images were acquired immediately after ligation (Day 0), seven or fourteen days after surgery. Images were analyzed using the moorFLPI-2 Review Software and recovery of blood perfusion was calculated as described above.

Vascular casting and micro computed tomography (CT) analysis

To visualize and quantitate the limb vasculature, we performed vascular casting, followed by microCT analysis[23]. For this, mice were given heparin (1000 units/mL; i.p.) as an anticoagulant and were subsequently sedated with sodium pentobarbital (50mg/kg). The heart was then cannulated with a 15G needle and mice were perfused systemically with adenosine (100 μmol/L; 10mL), followed by sodium nitroprusside (10 μmol/L) and then with bovine serum albumin (BSA; 0.05 % wt/vol) at a flow rate of 5 mL/min[19]. Undiluted Microfil (FlowTech, Inc.) was mixed with hardening solution, perfused, and allowed to solidify. The entire lower body was de-skinned and fixed in formalin for 24 h, which was followed by bone decalcification (Cal EX II) for 48 h. Samples were then imaged with a MicroCAT II (Siemens) scanning at 80 kVp and 500 μA, with 2×2 binning for a pixel resolution of 1024×1024 with 34 μm voxel sizes. After thresholding of soft tissue, casted blood vessel voxel volumes were then quantified using Analyze (AnalyzeDirect). For whole-mount imaging of Microfil casted limbs, harvested limbs were placed in graded solutions of glycerol (40%, 60%, 80%, 100%; changed every 24 hours) and images were acquired using a digital CCD camera (Nikon).

Histological analysis of ischemic limbs

For histological analysis, mice undergoing HLI for 14 days were euthanized and their limbs were dissected. The hamstring muscles were excised and fixed in formalin and paraffin-embedded. Three transverse cross sections of the muscles were mounted per slide and 2 slides were analyzed per mouse. Gross examination of tissue injury was performed on hematoxylin and eosin (H&E) stained sections. The number of myocytes with centrally-located nuclei indicates muscle regeneration and this was used to assess the extent of limb damage and recovery with RvD2 treatment[24]. Five to ten low power fields were examined in each section and the total number of myocytes with centrally located nuclei was determined and expressed as a % of the total myocytes per field.

Human peripheral artery disease cohort

Peripheral artery disease (PAD) patients with stable intermittent claudication, as well as healthy control subjects, were recruited as part of a prospective clinical trial investigating the effect of exercise training on skeletal muscle metabolism in PAD. The human study was approved by the IRB (#2010P001107) at Brigham and Women's Hospital and all subjects gave signed informed consent. The diagnosis of PAD was made based on a resting ankle-brachial index (ABI) of ≤0.90 and/or a decrease in ABI of at least 20% following maximal exercise. Patients with diabetes mellitus and those with signs of critical limb ischemia were excluded. To minimize risk of bleeding during the calf muscle biopsy, subjects were also excluded if they were taking warfarin. Healthy subjects were at least 50 years of age, had no known medical problems, and were ineligible if they had smoked within the past year. Subjects were recruited from clinical practices at Brigham and Women's Hospital and by advertisement.

Biopsy specimens were obtained from the medial head of the gastrocnemius. For PAD subjects, samples were taken from the more symptomatic leg or the leg with a lower ABI if the subject experienced equal bilateral symptoms. Under local anesthesia, approximately

100-150 mg of muscle tissue was collected using a 5 mm Bergstrom percutaneous muscle biopsy needle. Samples were immediately frozen in liquid nitrogen and stored at −80°C. Calf muscle biopsy samples were obtained from 15 subjects with PAD that completed the study and 7 healthy age-matched controls. The complete results of this ongoing clinical study will be reported separately.

Solid phase extraction and LC-MS/MS identification of resolvins

To assess the formation of RvD2 and 17-HDHA, skeletal muscle biopsies from PAD patients or limb skeletal muscle tissues from mice undergoing HLI were collected and minced in ice-cold methanol. Bone marrow was isolated from femurs and tibias of mice undergoing HLI by flushing with ice-cold methanol. Prior to solid-phase extraction, internal deuterium-labeled standards (i.e., d_5-RvD2 and d_8-5*S*-HETE) were added to skeletal muscle, bone marrow and monocyte samples (see below) to assess extraction recovery. Solid phase extraction and LC-MS/MS analysis were carried out essentially as described in Colas *et. al*[25]. Briefly, lipid mediators were extracted using C18 solid phase extraction cartridges and an automated extraction system (RapidTrace, Biotage). Methyl formate fractions were collected and the solvent was evaporated using a stream of N_2 gas, followed by re-suspension in methanol:water (50:50). Samples were then analyzed by liquid chromatography-tandem mass spectrometry (LC-MS/MS) using a Poroshell reverse-phase C18 column (100 mm × 4.6 mm × 2.7 μm; Agilent Technologies) equipped high performance liquid chromatography system (HPLC; Shimadzu) coupled to a QTrap 5500 mass spectrometer (AB Sciex). The mobile phase consisted of methanol:water:acetic acid (55:45:0.01 vol/vol/vol) and was ramped to 85:15:0.01 (vol/vol/vol) over 10 min, followed by ramping to 98:2:0.01 (vol/vol/vol) over the next 8 min and held for additional 2 min. The entire sample elution was performed using a constant flow rate of 400 μL/min at a constant temperature of 50°C. The QTrap was operated in negative ionization mode using scheduled multiple reaction monitoring (MRM) and transitions for RvD2 (375>215; 375>175) and 17-HDHA (343>245) coupled with information-dependent acquisition (IDA) and enhanced product ion-scanning (EPI). Mediators were identified using retention time and six diagnostic MS/MS ions, as compared with identical authentic standards (Cayman Chemical). Concentration was determined using standard curves generated for each mediator with synthetic standards after normalization of extraction recovery based on internal standards.

Splenic monocyte isolation and *in vitro* stimulation

To obtain a pure population of splenic monocytes, intact spleens were rapidly excised from anesthetized WT or *Alox15*-deficient mice and ruptured between two microscope slides. The spleen was then rubbed through a 40 micron cell strainer and rinsed with Pharmlyse to lyse red blood cells. After 5 min incubation in the dark at room temperature, the strained cells were washed with PBS containing 2 mmol/L EDTA and 0.5% BSA (MACS buffer). An EasySep mouse Monocyte Enrichment Kit (Stemcell Technologies) was then used to deplete non-monocyte populations by antibody-biotin-magnetic bead separation. The remaining population was confirmed by flow cytometry to be approximately 93% pure Ly-$6C^+CCR2^+$ monocytes. After isolation of splenic monocytes, cells were washed with Hank's Balanced Salt Solution to remove EDTA and to supplement calcium. Monocytes were then divided (1

× 10^5 cells/incubation) and stimulated with calcium ionophore (A23187; 10 μmol/L) and docosahexaenoic acid (DHA; 10 μmol/L) for 30 min at 37°C. The incubation was then terminated with 1.5 mL of ice-cold methanol and the samples were immediately frozen at −80°C for subsequent LC-MS/MS analysis (see above).

Flow cytometry analysis of leukocytes in ischemic limbs

To identify leukocyte populations in muscle tissue, HLI was carried out at as described above and mice were euthanized after 3 days. The right hamstring muscles of the upper limb were then excised, weighed, and placed in enzyme digestion solution consisting of 500 U/mL collagenase II and 2.5 U/mL dispase II in 1800 μL of Hank's Balanced Salt Solution. Muscles were left to digest at 37°C for 1.5 h. The digestate was then strained through a 40 micron cell strainer and washed with 2 mL of PBS with 1% BSA. The strained cells were incubated with Fc-block (anti-CD16/32) and then stained with FITC anti-CCR2, APC anti-F4/80, APC/Cy7 anti-Ly-6G, and PerCP anti-CD45. After 30 min, cells were washed with 1mL of PBS-BSA and analyzed using a BD LSR II flow cytometer and FlowJo software.

Multiplex ELISA analysis of mouse plasma

Mouse peripheral blood was collected by cardiac puncture, anti-coagulated with EDTA and centrifuged at 2000*x g* for 20 min. The plasma supernatant was collected and frozen at −80°C. Multiplex ELISA analyses were then performed by Quansys Biosciences.

Matrigel plug angiogenesis assay

To quantify angiogenesis, we used the Matrigel plug assay[23]. A 500 μL aliquot of Matrigel (Cultrex HC, Trevigen) was thawed on ice and mixed with either no additives, 50 U heparin + bFGF (500 ng), or RvD2 (100 ng). The mixture was then loaded into syringes with an attached 25-gauge needle. Mice were anesthetized with isoflurane and hair was removed with depilatory cream on the right lateral abdomen. The Matrigel mixture was then injected subcutaneously and solidified into plugs over 20 min. After 7 days, mice were euthanized and the Matrigel plugs were excised. To release the infiltrated endothelial cells, Matrigel plugs were digested with 5 mg/mL of Type I and II collagenase in 1 mL of Hank's Balanced Salt Solution for 1 hour at 37°C. Digested plugs were then strained with a 40 micron cell strainer and rinsed with PBS-BSA. The cell solution was incubated with Fc-block (anti-CD16/32) and then stained with PE anti-CD31 and PE/Cy7 anti-CD105. The cells were analyzed by flow cytometry as described above.

Endothelial cell migration and proliferation assays

To assess migration, mouse endothelial cells (MS1; ATCC) were seeded at 1 × 10^6 cells per well the night prior to experimentation in 3 mL of Dulbecco's Modified Eagle Medium (DMEM). Using a 200 μL pipette tip, two vertical scratches were made across the culture dish. The scratch was then imaged and the medium was replaced with fresh media containing VEGF-A (100 ng/mL) or RvD2 (0.1-10 nmol/L). In some experiments, the cells were pre-incubated with Rac inhibitor, NSC23766 (100 nmol/L), pertussis toxin (PTX; 1μg/mL), L-NAME (100μmol/L) or *O*-1918 (20 μmol/L) 30 min prior to stimulation with RvD2 (10 nmol/L). Eighteen hours later, the plates were imaged again. The 0 h and 18 h images

were then processed by Photoshop (Adobe) with vertical lines demarcating migration of cells into the scratch site, and the width was determined using Image J (NIH). To assess proliferation, MS1 cells were seeded at 1×10^4 cells per well in 100 μL of DMEM containing 1% FBS overnight. The next morning, cells were given fresh media containing VEGF-A (100 ng/mL) or RvD2 (0.1-10 nmol/L) and incubated at 37°C for 48 h. Cell proliferation was measured using a Click-iT EdU kit (Life Technologies) and quantitated on a microplate reader (Biotek), while viability and total cell number were determined in separate assays using an MTT assay kit (Invitrogen). For qRT-PCR analysis, cells were stimulated with or without VEGF-A (100 ng/mL) for 24 hours then lysed with RLT buffer containing 2-mercaptoethanol and processed as described below.

Assessment of vascular permeability

Vascular permeability was assessed *in vivo* using a modified Miles assay[26, 27]. As with previous surgical procedures, mice were anesthetized with 2% isoflurane (2 L/min O_2) and maintained on a temperature controlled water blanket at 37°C. The dorsal skin was shaved and the hair was removed with depilatory cream. Evan's blue dye was administered by retro-orbital injection (100 μl, 1% in PBS) and after 5 min, 20 μl of PBS, histamine (25 ng/μl) or RvD2 (5 ng/μl) was injected subcutaneously into the dorsal skin. Mice were euthanized after 10 min by cervical dislocation and the dorsal skin was removed. The injection sites were collected using a 12 mm biopsy punch and incubated in formamide at 55°C for 24h. Evan's blue extravasation into the tissue was measured by absorption at 620 nm using a Nanodrop (Thermo) and is expressed as μg of Evan's blue dye per cm^2 of skin.

Quantitative RT-PCR analysis

Mouse hamstring muscles were harvested, snap-frozen in liquid N_2 and pulverized. The pulverized tissue was incubated and vortexed in TRIzol (Life Technologies) for 5 min. Tissue homogenates were then incubated with chloroform for 3 min and then centrifuged at 12,000 × *g* for 15 min at 4°C. The upper aqueous phase was transferred to a new tube and RNA was then purified with an RNeasy kit (Qiagen). Similarly, RNA from cell lysates collected in RLT buffer was purified with an RNeasy kit and RNA quality was checked by 260/280 UV absorbance ratio with a Nanodrop (Thermo). cDNA was prepared by PCR using AMV reverse transcriptase and oligoDT primers. Real-time amplification was performed with PerfeCTa SYBR Green FastMix (Quanta Biosciences) using a 7900HT Fast Real-time PCR system (Applied Biosystems). Commercially available primers were used for targeted analysis of *Emr1* or *Gpr18* (SA Biosciences). The hypoxanthine-guanine phosphoribosyl transferase (*Hprt*) housekeeping gene was used as internal quantitation control. Relative expression was calculated using the $2^{-\Delta\Delta Ct}$ method.

Rac activation assay and Western blotting

MS1 cells were cultured on 150 mm plates in 30 mL of DMEM with 10% FBS until 50% confluence. Culture media was then changed to 1% serum DMEM for 18 hours. Cells were either left unstimulated or stimulated with RvD2 (1 nmol/L) for 30 min. Plates were then rinsed with ice-cold PBS to halt the reaction. An activated GTP-bound Rac pull-down assay was performed using a Rac activation kit (Cell Biolabs). Subsequently, Rac pull-down samples were separated by SDS-PAGE and transferred to polyvinylidene difluoride (PVDF)

membranes. The membrane was blocked overnight in tris-buffered saline with 1% tween 20 (TBS-T) and 5% powdered milk. Total Rac was then probed with anti-Rac antibodies (Cell Signaling Technologies) and anti-rabbit-HRP in TBS-T with 1% BSA. Membranes were then developed with HRP substrate (Millipore) and scanned with a Typhoon bioimager (GE Healthcare). Densitometry analysis was performed using ImageJ.

The abundance of GPR18 protein in endothelial cells was measured by Western blot analysis. For this, confluent MS1 cells were lysed in RIPA buffer with protease and phosphatase inhibitor cocktails (ThermoFisher Scientific) added. Samples were prepared at a concentration of 50 ug of protein in sample buffer with 100 mM DTT, then separated by SDS-PAGE and transferred to a PVDF membrane. The membrane was blocked in TBS-T and 5% milk for 2 hours at room temperature and incubated overnight at 4° C in TBS-T and 5% milk with the primary anti-GPR18 (Abcam 174835) antibody. The secondary anti-rabbit-HRP (Cell Signaling) antibody was incubated in TBS-T and 5% milk at room temperature for 1.5 hours. The blot was then developed using Luminata Forte (EMD Millipore) and X-ray film.

Statistics

Data are presented as mean ± standard error of the mean (SEM). Parametric statistical analysis was performed in cases where cumulative data was normally distributed, as determined by D'Augostino & Pearson omnibus normality tests. Based on this, we assumed a normal distribution in individual assays of the same type but with smaller sample sizes. For this, multiple groups were compared using one-way ANOVA, followed by Tukey's (comparing all groups) or Dunnett's (comparing treatments vs. control group) post-tests for contrasts of interest. For perfusion recovery, two-way ANOVA was performed, followed by Sidak's multiple comparisons post-tests. For direct comparisons, an unpaired two-tailed Student's *t* test was used. In individual assays where normality could not be tested based on sample size without cumulative historical data, we used nonparametric Kruskal-Wallis tests, with Dunn's multiple comparisons post-tests (comparing all groups) as indicated in the figure legends. In all cases, a $P<0.05$ was considered significant; exact P values for significant relationships are indicated in the figures. GraphPad Prism 6.0 was used for all statistical analysis.

Results

RvD2 is generated in ischemic tissue in both mice and humans

In acute sterile or infectious inflammation, D-series resolvins are generated by leukocytes during the resolution phase[14]. Their biosynthesis involves conversion of docosahexaenoic acid (DHA) to a 17-hydroperoxide (17-H(p)DHA) intermediate by 12/15-lipoxygenase (*Alox15*; 15-LOX type 1 in humans) (Figure 1A)[14-16]. This intermediate is further converted to RvD2 by 5-LOX (Figure 1A). Because ischemia stimulates mobilization of immune cells from bone marrow that promote revascularization[28], we first questioned whether RvD2 is generated in the bone marrow during ischemia. Indeed, we observed that RvD2 and its biosynthetic pathway marker, 17-hydroxyDHA (17-HDHA), were generated in the ischemic limb bone marrow as early as 24h post-surgery (Figure 1B). Representative MS/MS spectra

of 17-HDHA and RvD2 are shown in Figure 1C. The production of RvD2 in bone marrow preceded its appearance in ischemic skeletal muscle; by day 5, levels of RvD2 were significantly increased in mice undergoing HLI as compared with day 3 (Figure 1D). The increase in the production of RvD2 in skeletal muscle at day 5 was inversely related to its biosynthetic intermediate, 17-HDHA. Importantly, we also identified RvD2 in skeletal muscle biopsies from peripheral artery disease (PAD) patients, whereas RvD2 was absent in skeletal muscle of healthy individuals (Figure 1E and F).

Monocytes play an essential role in revascularization during HLI, hence we asked whether they are a cellular source of RvD2. We found that $CCR2^{+}$ monocytes are recruited to skeletal muscle during HLI (day 3; Figure 1G). Splenic monocytes converted DHA to 17-HDHA and RvD2 (Figure 1H). This conversion was essentially abolished in monocytes isolated from *Alox15*$^{-/-}$ mice (Figure 1H), validating their enzymatic biosynthesis. Collectively, these results show that RvD2 is generated in a temporal manner during HLI and that monocytes are a potential cellular source of RvD2 during HLI[29].

Tissue perfusion and arteriogenesis are enhanced by RvD2 during HLI

Given that RvD2 was generated in a temporal manner during HLI, we next asked whether therapeutic administration of RvD2 could enhance perfusion recovery. Previous studies have shown that exogenous RvD2 is effective at resolving inflammation *in vivo* at picogram-nanogram doses[16, 30]. We began treatment at day 1, preceding its endogenous biosynthesis in skeletal muscle (see Figure 1). Using laser Doppler perfusion imaging, mice undergoing HLI and treated with vehicle showed a time-dependent increase in tissue perfusion that reached ~30% restoration of blood flow by day 14 post-HLI (Figure 2A, B). In contrast, mice treated with RvD2 showed significant improvement in perfusion that manifested by day 7 (Figure 2B). We visualized the limb vasculature using Microfil casting and microCT. For this, we first used a milder model of HLI to limit endogenous arteriogenesis (see scheme; Figure 2C). Whole-mount imaging of vascular-casted limbs indicated that in comparison with vehicle treatment, RvD2 increased the appearance of enlarged collateral vessels (Figure 2C). Quantification of vascular volume by microCT analysis revealed a significant increase by RvD2 (Figure 2D). In a more severe model of HLI that stimulates robust endogenous arteriogenesis (see scheme in Figure 2E), we found that RvD2 significantly enhanced vascular volume (Figure 2F) and the appearance of corkscrew-like collateral vessels (Figure 2E; indicated by white arrows). Collectively, these results show that RvD2 enhances perfusion during HLI, likely by increasing arteriogenesis.

RvD2 resolves inflammation and promotes tissue regeneration during revascularization

During acute inflammation, RvD2 hastens resolution by reducing neutrophil recruitment and pro-inflammatory cytokine production, as well as by enhancing macrophage efferocytosis (clearance of apoptotic cells)[16, 30]. Because most pro-revascularization mediators also enhance inflammation, we next sought to determine how exogenous RvD2 modulates the sterile inflammatory response during HLI. In comparison with sham controls, levels of neutrophils ($Ly6G^{+}F4/80^{-}$) increased significantly in skeletal muscle of mice undergoing HLI (Figure 3A-C). This increase was prevented in mice treated with RvD2, consistent with its defined role in regulating neutrophil trafficking (Figure 3A-C). In contrast, RvD2 did not

affect tissue accumulation of monocytes or F4/80$^+$ macrophages, which play important roles in revascularization and tissue repair (Figure 3D, E and data not shown)[21, 31]. Consistent with the flow cytometry results, mRNA expression of *Emr1* (which encodes F4/80) was not affected by RvD2 in skeletal muscle of mice subjected to HLI (Figure 3F). Interestingly, RvD2 significantly decreased ischemia-induced increases in GM-CSF, and pro-inflammatory cytokine, TNFα (Figure 3G). These early changes in inflammation and revascularization translated into markedly enhanced tissue regeneration in ischemic skeletal muscle, as evidenced by a significant increase in myocytes with centrally-located nuclei at 14 days post-HLI (Figure 3H, I). These results indicate that RvD2 promotes the resolution of inflammation and tissue regeneration during HLI.

RvD2 stimulates endothelial cell migration in a receptor and Rac-dependent manner

We previously reported that RvD2 regulates leukocyte:endothelial interactions in part via direct actions on endothelial cells, which are important contributors to arteriogenesis[16, 32]. Here, we found that RvD2 enhanced endothelial cell migration in a concentration-dependent manner and to an extent similar to VEGF (Figure 4A and B). In contrast, RvD2 did not enhance endothelial cell proliferation, which was robustly stimulated by VEGF (Figure 4C). This lack of effect on proliferation was not due to a decrease in cell viability (Figure 4D). Matrigel plugs loaded with basic fibroblast growth factor (bFGF) showed a gross appearance consistent with angiogenesis, whereas control and RvD2-loaded plugs were essentially devoid of these structures (Figure 4E). Flow cytometry analysis of digested Matrigel demonstrated that bFGF significantly increased the accumulation of CD31$^+$CD105$^+$ (endoglin$^+$) cells[33], whereas their levels in RvD2-loaded plugs were not elevated above the control group indicating that RvD2 does not stimulate angiogenesis (Figure 4F, G).

Some vasoactive mediators that regulate endothelial migration can also promote vascular permeability (e.g., VEGF), thus, we assessed whether this process was affected by RvD2. As shown in Figure 4H, subcutaneous administration of RvD2 at the same dose used for HLI studies (see above) did not promote leakage of Evan's blue dye, whereas histamine markedly increased dye extravasation. These results, which are consistent with our prior studies using intravital microscopy[16], suggest that RvD2 modulates endothelial cell function without increasing vascular permeability.

Because RvD2 stimulated endothelial cell migration, we evaluated expression of its recently characterized specific receptor, GPR18[30]. Indeed, GPR18 (both protein and mRNA) was expressed in endothelial cells (Figure 5A, B) and *Gpr18* mRNA increased significantly upon treatment with VEGF for 24h (Figure 5B). Stimulation of migration by RvD2 was completely abolished in cells pretreated with pertussis toxin (PTX; Figure 5C) and by specific GPR18 antagonist, *O*-1918[34] (Figure 5D). To identify mediators of RvD2 action, we examined Rho-GTPases, which play an important role in endothelial cell migration[35] and are stimulated in macrophages by LXA_4, another pro-resolving lipid mediator[36]. RvD2 significantly increased the amount of active, GTP-bound Rac (Figure 5E), and the pro-migratory effects of RvD2 were blocked with Rac inhibitor, NSC23766[37] (Figure 5F). Consistent with our previous results showing that RvD2 stimulates the production of nitric oxide (NO) in human endothelial cells and that these effects are PTX sensitive[16], NOS

inhibitor, L-NAME, also blocked RvD2's pro-migratory actions (Figure 5F). Given the interplay between Rac and eNOS in regulating endothelial cell migration[38], these results suggest that RvD2 could affect migration by targeting the Rac/eNOS pathway.

Deficiency of RvD2 receptor, *Gpr18*, impairs perfusion during HLI

Our results demonstrate that, in addition to neutrophils and macrophages[30], GPR18 is expressed in endothelial cells; we next evaluated whether genetic deficiency of *Gpr18* affects perfusion recovery during HLI. As shown in Figure 6A, *Gpr18*-deficient mice had a marked endogenous defect in perfusion recovery during HLI, as compared with their WT littermates. Quantification of perfusion recovery showed that *Gpr18*-deficient mice recovered at a slower rate than their WT littermates and had significant defects in perfusion that manifested by day 7 post-HLI (Figure 6B and C). The defect in perfusion in *Gpr18*-deficient mice was not due to differences in limb perfusion at baseline.

RvD2 rescues defective revascularization in obese-diabetic mice

Chronic inflammation and metabolic disease impair the normal process of tissue revascularization and diabetics are particularly susceptible to impaired tissue perfusion and wound healing[1, 2]. Moreover, diabetics with PAD have higher rates of vein graft failure[39]. In animal models of diabetes, revascularization and arteriogenesis during HLI are impaired[40, 41]. Thus, to test the translational relevance of our findings, we questioned whether RvD2 treatment could restore defective revascularization in diabetic mice. In comparison with WT mice, obese-diabetic mice (*db/db*) had a significant and sustained defect in revascularization during HLI (Figure 7). Treatment with RvD2 significantly increased tissue perfusion in *db/db* mice compared with vehicle treated mice and to a level that was indistinguishable from WT mice by day 14 (Figure 7). These results demonstrate that, in addition to enhancing the rate of normal revascularization, RvD2 overcomes defective perfusion recovery in diabetes.

Discussion

In this study, we found that RvD2 is generated in limb ischemia in both rodents and humans and that therapeutic administration of RvD2 enhances revascularization, while at the same time resolving inflammation. We identified the newly characterized receptor for RvD2 (i.e., GPR18) in endothelial cells and found that RvD2 stimulates endothelial cell migration in a Rac-dependent manner. Taken together, these findings assign a new biological role to RvD2 in the revascularization program and could open up new directions for the development of novel therapeutic interventions for patients with PAD and CLI.

During infection, tissue injury, or ischemia, the inflammatory response is tightly coupled to the wound-healing program; immune cells combat pathogens and clear cellular debris to enable subsequent stages of tissue repair and regeneration. In this process, monocytes and macrophages are particularly important because they produce growth factors and other mediators that regulate cell migration, proliferation and extracellular matrix remodeling[42]. Monocytes are mobilized from the bone marrow and the spleen during ischemia, preceding their accumulation in ischemic tissues[28]. We observed that RvD2 is produced in the bone

marrow during ischemia and by isolated splenic monocytes in a lipoxygenase-dependent manner. Monocytes are necessary for revascularization during HLI[8] and we found that RvD2 is sufficient to increase revascularization. These results are consistent with a previous study demonstrating that genetic deficiency of *Alox15* impairs perfusion during HLI[43], although it should be noted that 12/15-LOX contributes to the biosynthesis of several other lipid mediators. Thus, in our study, we focused on direct actions of RvD2 and its receptor, GPR18, to understand the specific role of RvD2 in revascularization.

It is significant to point out that our results show that mediators that diminish inflammation can enhance revascularization. This is important because most previously identified interventions that promote revascularization also increase inflammation and atherosclerosis[11, 12]. For instance, administration of monocyte chemoattractant protein 1 (MCP1) promotes monocyte recruitment and arteriogenesis during HLI, but also increases monocyte infiltration into atherosclerotic lesions and enhances lesion formation[11]. In contrast, IL-10 is an anti-inflammatory cytokine that is protective in atherosclerosis, but impairs revascularization during ischemia[12, 44]. Our results challenge this paradigm by demonstrating that RvD2 both resolves inflammation and promotes revascularization. These findings lend further support to the notion that effects of resolving inflammation are distinct from anti-inflammatory interventions, which are immunosuppressive. Because lipid mediators like resolvins are immunomodulatory, they decrease the production of pro-inflammatory mediators, while enhancing host defense (e.g., macrophage phagocytosis of bacteria and apoptotic cells)[14]. Indeed, we found that RvD2 did not promote vascular permeability or macrophage accumulation in skeletal muscle, but reduced neutrophil accumulation and TNFα and GM-CSF production. These effects were associated with improved revascularization and enhanced skeletal muscle regeneration, suggesting that unlike anti-inflammatory drugs, RvD2 has a dual effect - diminishing inflammation and promoting wound healing. We note that similar to other recent studies[20, 21], we ligated both the artery and vein in order to prevent damaging the associated nerve and to preserve limb function. Ligating the vein in addition to the artery may change the duration or mechanisms of perfusion recovery. However, the extent of perfusion recovery determined in our study is similar to that observed by other groups in which only the artery is ligated[8, 40]. In future studies, it may be important to determine how RvD2 affects perfusion in contexts that more closely mirror impaired perfusion in humans (e.g., atherosclerosis), and to determine how long-term treatment with RvD2 regulates later phases of tissue remodeling.

Promotion of the resolution of inflammation by RvD2 overcomes a critical barrier to revascularization therapy, i.e., chronic inflammation, which in PAD impairs endogenous revascularization and limits the effectiveness of pro-revascularization therapies[7]. Indeed, several inflammatory mediators including TNFα, are associated with poor clinical outcomes in PAD[45]. Moreover, accumulating evidence indicates that resolvins may also reduce atherosclerosis and pathologic restenosis[17, 46, 47]. The notion that resolving inflammation is critical for promoting revascularization is supported by our previous observation that plasma levels of another pro-resolving mediator, 15-epi LXA_4, are inversely correlated with PAD severity (i.e., intermittent claudication vs. CLI) in humans[13, 48]. Moreover, several chronic inflammatory diseases, including diabetes, obesity and asthma are associated with impaired production of pro-resolving mediators[13, 49]. Our results demonstrating that RvD2 rescues

defective revascularization in diabetic mice are thus a significant step toward clinical translation. In future studies it will be important to determine whether impaired revascularization in conditions such as diabetes and PAD is causally related to an imbalance in pro-inflammatory vs. pro-resolving mediators and whether treatment with resolvins could be a clinically useful approach to promoting revascularization.

In addition to resolving inflammation, we found that RvD2 directly stimulates endothelial cell migration by activating Rac. We identified the RvD2 receptor, GPR18, on endothelial cells and found that GPR18 mediates the pro-migratory actions of RvD2. Interestingly, *Gpr18*-deficient mice had endogenous defects in revascularization. Thus, in addition to regulating leukocyte trafficking during acute inflammation[30], GPR18 may play a role in endothelial cell function. In further support of this concept, prior studies have determined that *Gpr18* is expressed in human endothelial cells and regulates activation of protein kinase B/AKT in a PTX-sensitive manner[50]. Moreover, RvD2 was recently found to stimulate AKT phosphorylation in human endothelial cells[51]. We note that, unlike growth factors, RvD2 did not stimulate endothelial cell proliferation, vascular permeability or angiogenesis. In fact, previous studies have shown that pathologic neovascularization is inhibited by resolvins[52]. This property of pro-resolving mediators could be particularly beneficial in the context of atherosclerosis and cancer, where angiogenesis could fuel disease progression.

In summary, the results of this study uncover a new role of resolvins in tissue revascularization following ischemic injury and suggest that resolution of inflammation is an important component of the revascularization program. Because impaired tissue vascularization is associated with chronic inflammation in diseases such as PAD and diabetes, these results could have important implications for revascularization therapy.

Acknowledgments

The authors thank Charles N. Serhan and Nan Chiang (Harvard Medical School and Brigham and Women's Hospital) for assistance with experiments involving the *Gpr18*-deficient mice.

Sources of Funding

This work was supported in part by NIH grants HL106173, GM095467 (M.S.) and GM103492 (A.B., M.S. and D.J.C.). J.H. is the recipient of a National Research Service Award from the National Heart, Lung and Blood Institute, NIH (HL116186).

References

1. Vartanian SM, Conte MS. Surgical intervention for peripheral arterial disease. Circulation research. 2015; 116:1614–28. [PubMed: 25908732]
2. Bonaca MP, Creager MA. Pharmacological treatment and current management of peripheral artery disease. Circulation research. 2015; 116:1579–98. [PubMed: 25908730]
3. Criqui MH, Aboyans V. Epidemiology of peripheral artery disease. Circulation research. 2015; 116:1509–26. [PubMed: 25908725]
4. Chilian WM, Penn MS, Pung YF, Dong F, Mayorga M, Ohanyan V, Logan S, Yin L. Coronary collateral growth--back to the future. Journal of molecular and cellular cardiology. 2012; 52:905–11. [PubMed: 22210280]
5. Faber JE, Chilian WM, Deindl E, van Royen N, Simons M. A brief etymology of the collateral circulation. Arteriosclerosis, thrombosis, and vascular biology. 2014; 34:1854–9.

6. Simons M, Eichmann A. Molecular Controls of Arterial Morphogenesis. Circulation research. 2015; 116:1712–1724. [PubMed: 25953926]
7. Cooke JP, Losordo DW. Modulating the vascular response to limb ischemia: angiogenic and cell therapies. Circulation research. 2015; 116:1561–78. [PubMed: 25908729]
8. Heil M, Ziegelhoeffer T, Wagner S, Fernandez B, Helisch A, Martin S, Tribulova S, Kuziel WA, Bachmann G, Schaper W. Collateral artery growth (arteriogenesis) after experimental arterial occlusion is impaired in mice lacking CC-chemokine receptor-2. Circulation research. 2004; 94:671–7. [PubMed: 14963007]
9. Jetten N, Donners MM, Wagenaar A, Cleutjens JP, van Rooijen N, de Winther MP, Post MJ. Local delivery of polarized macrophages improves reperfusion recovery in a mouse hind limb ischemia model. PloS one. 2013; 8:e68811. [PubMed: 23894348]
10. Kuwahara G, Nishinakamura H, Kojima D, Tashiro T, Kodama S. GM-CSF treated F4/80+ BMCs improve murine hind limb ischemia similar to M-CSF differentiated macrophages. PloS one. 2014; 9:e106987. [PubMed: 25202910]
11. van Royen N, Hoefer I, Bottinger M, Hua J, Grundmann S, Voskuil M, Bode C, Schaper W, Buschmann I, Piek JJ. Local monocyte chemoattractant protein-1 therapy increases collateral artery formation in apolipoprotein E-deficient mice but induces systemic monocytic CD11b expression, neointimal formation, and plaque progression. Circulation research. 2003; 92:218–25. [PubMed: 12574150]
12. Epstein SE, Stabile E, Kinnaird T, Lee CW, Clavijo L, Burnett MS. Janus phenomenon: the interrelated tradeoffs inherent in therapies designed to enhance collateral formation and those designed to inhibit atherogenesis. Circulation. 2004; 109:2826–31. [PubMed: 15197154]
13. Serhan CN, Chiang N, Dalli J. The resolution code of acute inflammation: Novel pro-resolving lipid mediators in resolution. Seminars in immunology. 2015; 27:200–15. [PubMed: 25857211]
14. Serhan CN. Pro-resolving lipid mediators are leads for resolution physiology. Nature. 2014; 510:92–101. [PubMed: 24899309]
15. Spite M, Serhan CN. Novel lipid mediators promote resolution of acute inflammation: impact of aspirin and statins. Circulation research. 2010; 107:1170–84. [PubMed: 21071715]
16. Spite M, Norling LV, Summers L, Yang R, Cooper D, Petasis NA, Flower RJ, Perretti M, Serhan CN. Resolvin D2 is a potent regulator of leukocytes and controls microbial sepsis. Nature. 2009; 461:1287–91. [PubMed: 19865173]
17. Merched AJ, Ko K, Gotlinger KH, Serhan CN, Chan L. Atherosclerosis: evidence for impairment of resolution of vascular inflammation governed by specific lipid mediators. FASEB journal : official publication of the Federation of American Societies for Experimental Biology. 2008; 22:3595–606. [PubMed: 18559988]
18. Norling LV, Dalli J, Flower RJ, Serhan CN, Perretti M. Resolvin D1 limits polymorphonuclear leukocyte recruitment to inflammatory loci: receptor-dependent actions. Arteriosclerosis, thrombosis, and vascular biology. 2012; 32:1970–8.
19. Limbourg A, Korff T, Napp LC, Schaper W, Drexler H, Limbourg FP. Evaluation of postnatal arteriogenesis and angiogenesis in a mouse model of hind-limb ischemia. Nature protocols. 2009; 4:1737–46. [PubMed: 19893509]
20. Kim JA, March K, Chae HD, Johnstone B, Park SJ, Cook T, Merfeld-Clauss S, Broxmeyer HE. Muscle-derived Gr1(dim)CD11b(+) cells enhance neovascularization in an ischemic hind limb mouse model. Blood. 2010; 116:1623–6. [PubMed: 20516368]
21. Takeda Y, Costa S, Delamarre E, Roncal C, Leite de Oliveira R, Squadrito ML, Finisguerra V, Deschoemaeker S, Bruyere F, Wenes M, Hamm A, Serneels J, Magat J, Bhattacharyya T, Anisimov A, Jordan BF, Alitalo K, Maxwell P, Gallez B, Zhuang ZW, Saito Y, Simons M, De Palma M, Mazzone M. Macrophage skewing by Phd2 haplodeficiency prevents ischaemia by inducing arteriogenesis. Nature. 2011; 479:122–6. [PubMed: 21983962]
22. Traktuev DO, Tsokolaeva ZI, Shevelev AA, Talitskiy KA, Stepanova VV, Johnstone BH, Rahmat-Zade TM, Kapustin AN, Tkachuk VA, March KL, Parfyonova YV. Urokinase gene transfer augments angiogenesis in ischemic skeletal and myocardial muscle. Mol Ther. 2007; 15:1939–46. [PubMed: 17653104]

23. Simons M, Alitalo K, Annex BH, Augustin HG, Beam C, Berk BC, Byzova T, Carmeliet P, Chilian W, Cooke JP, Davis GE, Eichmann A, Iruela-Arispe ML, Keshet E, Sinusas AJ, Ruhrberg C, Woo YJ, Dimmeler S, American Heart Association Council on Basic Cardiovascular S, Council on Cardiovascular S and Anesthesia. State-of-the-Art Methods for Evaluation of Angiogenesis and Tissue Vascularization: A Scientific Statement From the American Heart Association. Circulation research. 2015; 116:e99–132. [PubMed: 25931450]
24. Ciciliot S and Schiaffino S. Regeneration of mammalian skeletal muscle. Basic mechanisms and clinical implications. Current pharmaceutical design. 2010; 16:906–14. [PubMed: 20041823]
25. Colas RA, Shinohara M, Dalli J, Chiang N, Serhan CN. Identification and signature profiles for pro-resolving and inflammatory lipid mediators in human tissue. American journal of physiology Cell physiology. 2014; 307:C39–54. [PubMed: 24696140]
26. Miles AA, Miles EM. Vascular reactions to histamine, histamine-liberator and leukotaxine in the skin of guinea-pigs. J Physiol. 1952; 118:228–57. [PubMed: 13000707]
27. Mikelis CM, Simaan M, Ando K, Fukuhara S, Sakurai A, Amornphimoltham P, Masedunskas A, Weigert R, Chavakis T, Adams RH, Offermanns S, Mochizuki N, Zheng Y, Gutkind JS. RhoA and ROCK mediate histamine-induced vascular leakage and anaphylactic shock. Nat Commun. 2015; 6:6725. [PubMed: 25857352]
28. Swirski FK, Nahrendorf M. Leukocyte behavior in atherosclerosis, myocardial infarction, and heart failure. Science. 2013; 339:161–6. [PubMed: 23307733]
29. Mirakaj V, Dalli J, Granja T, Rosenberger P, Serhan CN. Vagus nerve controls resolution and pro-resolving mediators of inflammation. The Journal of experimental medicine. 2014; 211:1037–48. [PubMed: 24863066]
30. Chiang N, Dalli J, Colas RA, Serhan CN. Identification of resolvin D2 receptor mediating resolution of infections and organ protection. The Journal of experimental medicine. 2015; 212:1203–17. [PubMed: 26195725]
31. Arnold L, Henry A, Poron F, Baba-Amer Y, van Rooijen N, Plonquet A, Gherardi RK, Chazaud B. Inflammatory monocytes recruited after skeletal muscle injury switch into antiinflammatory macrophages to support myogenesis. The Journal of experimental medicine. 2007; 204:1057–69. [PubMed: 17485518]
32. Moraes F, Paye J, Mac Gabhann F, Zhuang ZW, Zhang J, Lanahan AA, Simons M. Endothelial cell-dependent regulation of arteriogenesis. Circulation research. 2013; 113:1076–86. [PubMed: 23897694]
33. Duff SE, Li C, Garland JM, Kumar S. CD105 is important for angiogenesis: evidence and potential applications. FASEB journal : official publication of the Federation of American Societies for Experimental Biology. 2003; 17:984–92. [PubMed: 12773481]
34. McHugh D, Hu SS, Rimmerman N, Juknat A, Vogel Z, Walker JM, Bradshaw HB. N-arachidonoyl glycine, an abundant endogenous lipid, potently drives directed cellular migration through GPR18, the putative abnormal cannabidiol receptor. BMC neuroscience. 2010; 11:44. [PubMed: 20346144]
35. Tzima E. Role of small GTPases in endothelial cytoskeletal dynamics and the shear stress response. Circulation research. 2006; 98:176–85. [PubMed: 16456110]
36. Maderna P, Cottell DC, Berlasconi G, Petasis NA, Brady HR, Godson C. Lipoxins induce actin reorganization in monocytes and macrophages but not in neutrophils: differential involvement of rho GTPases. The American journal of pathology. 2002; 160:2275–83. [PubMed: 12057930]
37. Gao Y, Dickerson JB, Guo F, Zheng J, Zheng Y. Rational design and characterization of a Rac GTPase-specific small molecule inhibitor. Proceedings of the National Academy of Sciences of the United States of America. 2004; 101:7618–23. [PubMed: 15128949]
38. Sawada N, Salomone S, Kim HH, Kwiatkowski DJ, Liao JK. Regulation of endothelial nitric oxide synthase and postnatal angiogenesis by Rac1. Circulation research. 2008; 103:360–8. [PubMed: 18599867]
39. Owens CD, Ho KJ, Conte MS. Lower extremity vein graft failure: a translational approach. Vascular medicine. 2008; 13:63–74. [PubMed: 18372442]
40. Schiekofer S, Galasso G, Sato K, Kraus BJ, Walsh K. Impaired revascularization in a mouse model of type 2 diabetes is associated with dysregulation of a complex angiogenic-regulatory network. Arteriosclerosis, thrombosis, and vascular biology. 2005; 25:1603–9.

41. van Golde JM, Ruiter MS, Schaper NC, Voo S, Waltenberger J, Backes WH, Post MJ, Huijberts MS. Impaired collateral recruitment and outward remodeling in experimental diabetes. Diabetes. 2008; 57:2818–23. [PubMed: 18633114]

42. Mantovani A, Biswas SK, Galdiero MR, Sica A, Locati M. Macrophage plasticity and polarization in tissue repair and remodelling. The Journal of pathology. 2013; 229:176–85. [PubMed: 23096265]

43. Singh NK, Kundumani-Sridharan V, Rao GN. 12/15-Lipoxygenase gene knockout severely impairs ischemia-induced angiogenesis due to lack of Rac1 farnesylation. Blood. 2011; 118:5701–12. [PubMed: 21841162]

44. Silvestre JS, Mallat Z, Duriez M, Tamarat R, Bureau MF, Scherman D, Duverger N, Branellec D, Tedgui A, Levy BI. Antiangiogenic effect of interleukin-10 in ischemia-induced angiogenesis in mice hindlimb. Circulation research. 2000; 87:448–52. [PubMed: 10988235]

45. Pande RL, Brown J, Buck S, Redline W, Doyle J, Plutzky J, Creager MA. Association of monocyte tumor necrosis factor alpha expression and serum inflammatory biomarkers with walking impairment in peripheral artery disease. Journal of vascular surgery. 2015; 61:155–61. [PubMed: 25095746]

46. Akagi D, Chen M, Toy R, Chatterjee A, Conte MS. Systemic delivery of proresolving lipid mediators resolvin D2 and maresin 1 attenuates intimal hyperplasia in mice. FASEB journal : official publication of the Federation of American Societies for Experimental Biology. 2015; 29:2504–13. [PubMed: 25777995]

47. Hasturk H, Abdallah R, Kantarci A, Nguyen D, Giordano N, Hamilton J, Van Dyke TE. Resolvin E1 (RvE1) Attenuates Atherosclerotic Plaque Formation in Diet and Inflammation-Induced Atherogenesis. Arteriosclerosis, thrombosis, and vascular biology. 2015; 35:1123–33.

48. Ho KJ, Spite M, Owens CD, Lancero H, Kroemer AH, Pande R, Creager MA, Serhan CN, Conte MS. Aspirin-triggered lipoxin and resolvin E1 modulate vascular smooth muscle phenotype and correlate with peripheral atherosclerosis. The American journal of pathology. 2010; 177:2116–23. [PubMed: 20709806]

49. Spite M, Claria J, Serhan CN. Resolvins, specialized proresolving lipid mediators, and their potential roles in metabolic diseases. Cell metabolism. 2014; 19:21–36. [PubMed: 24239568]

50. Offertaler L, Mo FM, Batkai S, Liu J, Begg M, Razdan RK, Martin BR, Bukoski RD, Kunos G. Selective ligands and cellular effectors of a G protein-coupled endothelial cannabinoid receptor. Molecular pharmacology. 2003; 63:699–705. [PubMed: 12606780]

51. Maekawa T, Hosur K, Abe T, Kantarci A, Ziogas A, Wang B, Van Dyke TE, Chavakis T, Hajishengallis G. Antagonistic effects of IL-17 and D-resolvins on endothelial Del-1 expression through a GSK-3beta-C/EBPbeta pathway. Nat Commun. 2015; 6:8272. [PubMed: 26374165]

52. Connor KM, SanGiovanni JP, Lofqvist C, Aderman CM, Chen J, Higuchi A, Hong S, Pravda EA, Majchrzak S, Carper D, Hellstrom A, Kang JX, Chew EY, Salem N Jr. Serhan CN, Smith LE. Increased dietary intake of omega-3-polyunsaturated fatty acids reduces pathological retinal angiogenesis. Nature medicine. 2007; 13:868–73.

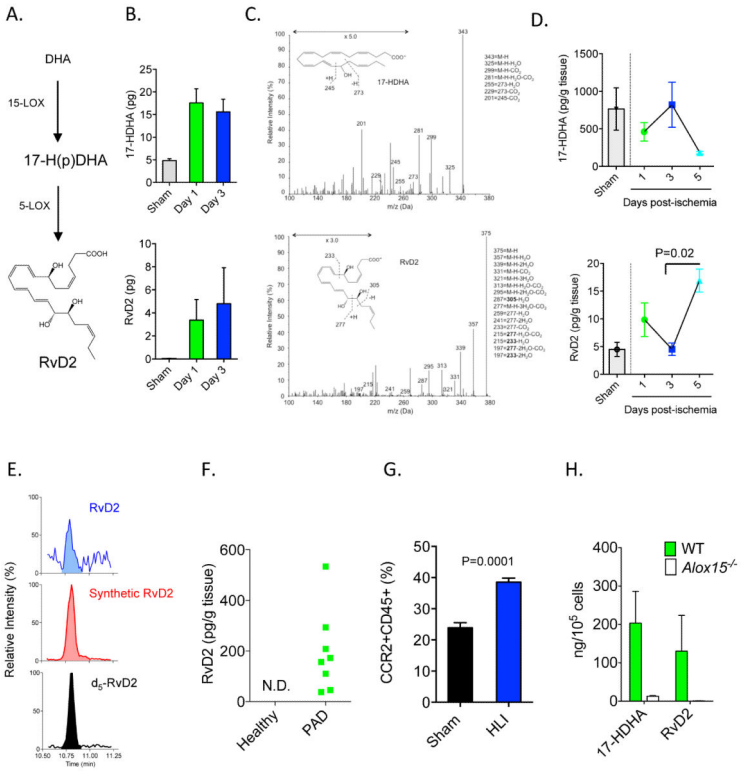

Figure 1. Biosynthesis of RvD2 in mice undergoing HLI and humans with peripheral artery disease

(A) Schematic of the RvD2 biosynthetic pathway, where docosahexaenoic acid (DHA) is converted to a 17-hydroperoxide (Hp) intermediate by 12/15-lipoxygenase (Alox15; 15-LOX type 1 in humans). This intermediate is converted to RvD2 by 5-LOX. (B) Quantification of 17-HDHA and RvD2 in bone marrow of mice undergoing sham surgery or HLI. (C) Representative MS/MS spectra of 17-HDHA and RvD2 generated in bone marrow during HLI (day 3), with structure and diagnostic ion assignments shown as inset. (D) Time course of 17-HDHA and RvD2 formation in skeletal muscle of mice undergoing HLI. (E) Representative multiple reaction monitoring (MRM) chromatogram used for identification of RvD2 in skeletal muscle biopsies of peripheral artery disease (PAD) patients, with external RvD2 standard and internal deuterium labeled (d_5) RvD2 standard shown (retention time: 10.8 min). (F) Quantification of RvD2 in PAD patients and healthy controls (N.D.: Not detected). (G) Flow cytometry analysis of $CCR2^+CD45^+$ monocytes in skeletal muscle of mice undergoing HLI (day 3; % of total cell gate). (H) Biosynthesis of 17-HDHA and RvD2 in splenic $CCR2^+$ monocytes isolated from WT or *Alox15*$^{-/-}$ mice. Data are mean ± SEM; n=6-7/group/time point (B, C), n=3 (sham) and n=4-7/group/time point (D), 7 (healthy) or 15 (PAD)/group (F), and n=3-5/group (G, H). Statistical comparisons were made using nonparametric one-way ANOVA (Kruskal-Wallis), followed by Dunn's multiple comparisons post-tests (D) or by an unpaired two-tailed Student's *t* test (G).

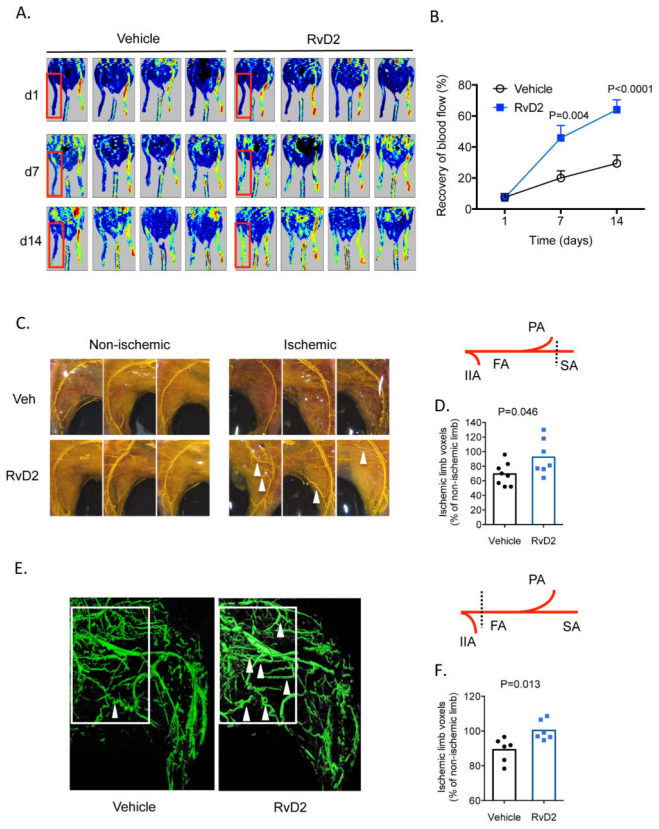

Figure 2. RvD2 enhances arteriogenesis during HLI

(A, B) Laser Doppler perfusion imaging of mice undergoing HLI and treated with vehicle or RvD2 for 14 days (d). Quantification of tissue perfusion in the ischemic limb (red box), presented as % perfusion of the non-ischemic limb is shown in (B). (C) Representative whole-mount images of Microfil vascular casted limbs of mice undergoing HLI and treated with vehicle or RvD2 for 3 days. A schematic of the ligation site is shown in the right panel; IIA: internal iliac artery; FA: femoral artery; PA: popliteal artery; SA: saphenous artery. (D) Quantification of vascular volume by microCT analysis. (E) Representative microCT images showing the limb vasculature in mice undergoing HLI and treated with vehicle or RvD2 for 7 days. The white box indicates the region of interest with identification of corkscrew-like collateral vessels indicted by arrowheads. This more severe (proximal) ligation site is indicated in the schematic in the right panel. (F) Quantification of vascular volume by microCT analysis. Data are mean ± SEM; n=6-8/group. Statistical comparisons were made using a two-way ANOVA, followed by Sidak's multiple comparisons post-tests (B) or an unpaired two-tailed Student's *t* test (D, F)

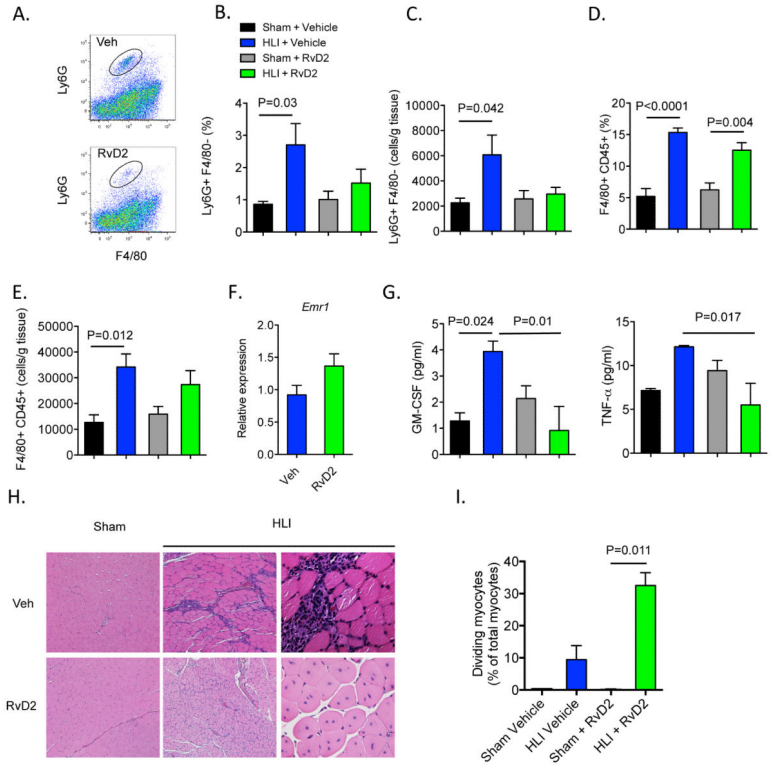

Figure 3. Therapeutic administration of RvD2 decreases inflammation and promotes tissue regeneration during HLI

(A) Representative flow cytometry dot plots of $Ly6G^{+}F4/80^{-}$ neutrophils in mice undergoing HLI and treated with vehicle or RvD2. Quantification by flow cytometry of $Ly6G^{+}$ neutrophils (B, C) and $F4/80^{+}CD45^{+}$ macrophages (D, E) in skeletal muscle isolated from mice undergoing sham surgery or HLI (day 3) and treated with vehicle or RvD2. Results are presented as a % of total cells and total cells/g of tissue. (F) Expression of *Emr1* (F4/80) in skeletal muscle of mice undergoing HLI and treated with vehicle or RvD2. (G) Plasma levels of GM-CSF and TNFα in mice undergoing sham surgery or HLI and treated with vehicle or RvD2. (H) Representative images (Hematoxylin and Eosin; 10x images left and middle panels; 40x far right panels) of skeletal muscle from mice undergoing sham surgery or HLI (day 14) and treated with vehicle or RvD2. (I) Quantification of myocytes with centrally-located nuclei in skeletal muscle. Data are mean ± SEM; n=4-5/group. Multiple group comparisons were made using one-way ANOVA, followed by Tukey's multiple comparisons post-tests (B-G) or non-parametric one-way ANOVA (Kruskal-Wallis), followed by Dunn's multiple comparisons post-tests (I).

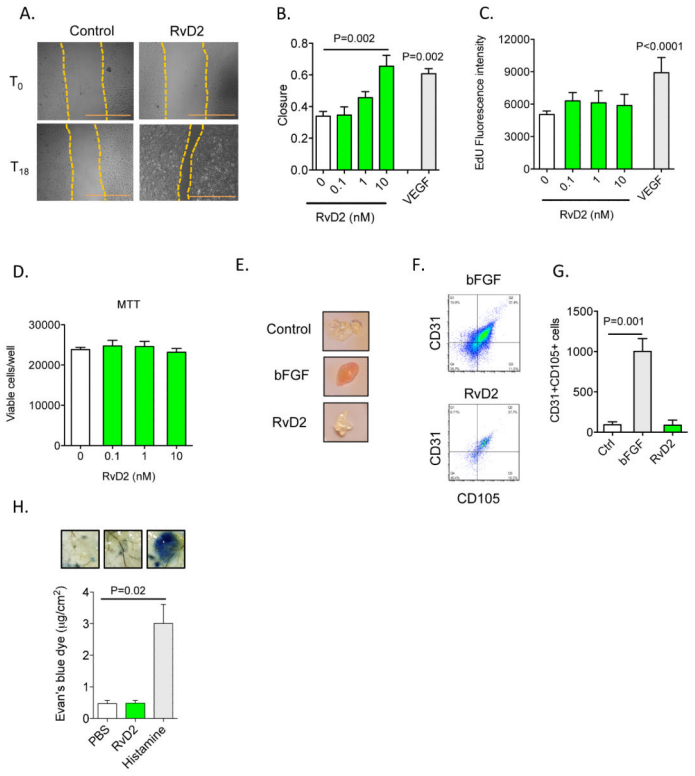

Figure 4. RvD2 stimulates endothelial cell migration but not proliferation

(A, B) Representative images (scale bar =1mm) and quantification of endothelial cell migration in response to vehicle, RvD2 or VEGF-A (100 ng/mL). (C) Proliferation assay (5-ethynyl-2'-deoxyuridine; EdU incorporation) of endothelial cells stimulated with RvD2 at indicated concentrations. (D) Endothelial cell viability (MTT assay) in the presence of RvD2. (E) Representative images of Matrigel plugs loaded with RvD2 or bFGF and excised from mice 7 days after implantation. (F) Flow cytometry dot plots of $CD31^{+}CD105^{+}$ ($endoglin^{+}$) cells isolated from Matrigel plugs as in F. (G) Quantification of $CD31^{+}CD105^{+}$ cells excised from Matrigel plugs. (H) Assessment of vascular permeability (Evan's blue dye extravasation) in mice given PBS, RvD2 or Histamine, with representative images of subcutaneous tissue biopsies shown. Data are mean ± SEM; n=3-6/group (A-G); n=4-6/group (H). Statistical comparisons were made using one-way ANOVA, followed by Dunnett's multiple comparisons post-tests (compared with control; B, C, D & G), non-parametric one-way ANOVA, followed by Dunn's multiple comparisons post-tests (H), or an unpaired two-tailed Student's *t* test (VEGF vs. Control; B, C).

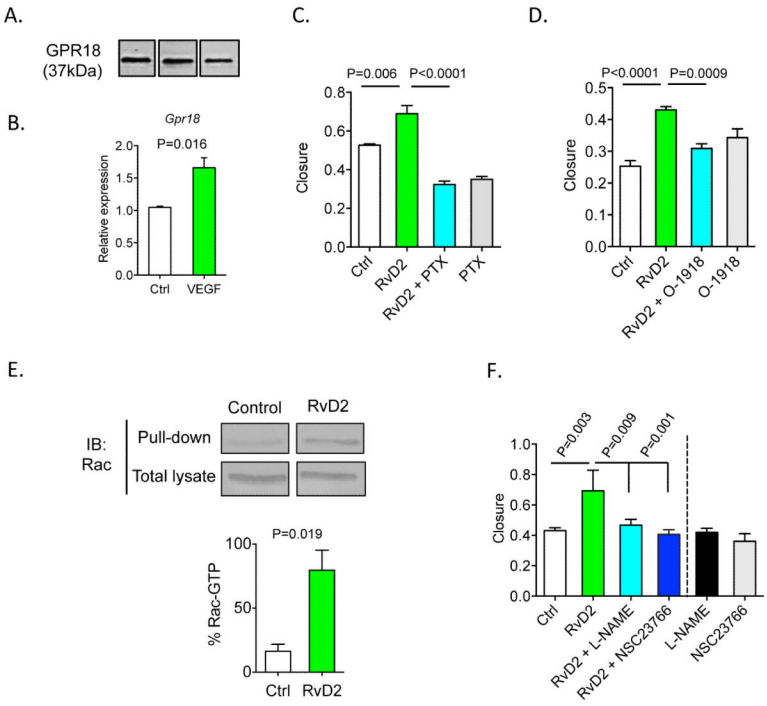

Figure 5. RvD2 promotes endothelial cell migration in a GPR18 and Rac-dependent manner

(A) Western blot of GPR18 (37kDa) in endothelial cells. (B) Levels of *Gpr18* transcripts in endothelial cells stimulated with VEGF-A (100 ng/mL) for 24h. (C, D) Migration of endothelial cells stimulated with RvD2 (10 nmol/L) in cells pre-treated with pertussis toxin (PTX; 1 μg/mL) or GPR18 inhibitor (*O*-1918; 20 μmol/L). (E) Rac activation assay in endothelial cells stimulated with RvD2 (1 nM; 30 min), with quantification of GTP-bound Rac shown in the lower panel. (F) Quantification of endothelial cell migration in cells pre-treated with Rac inhibitor, NSC23766 (100 μmol/L) or nitric oxide synthase inhibitor, L-NAME (100μmol/L), and then stimulated with RvD2 (10 nmol/L). Data are mean ± SEM; n=3-6/group. Statistical comparisons were made using one-way ANOVA, followed by Tukey's multiple comparisons post-tests (C, D, F) or an unpaired two-tailed Student's *t* test (B, E).

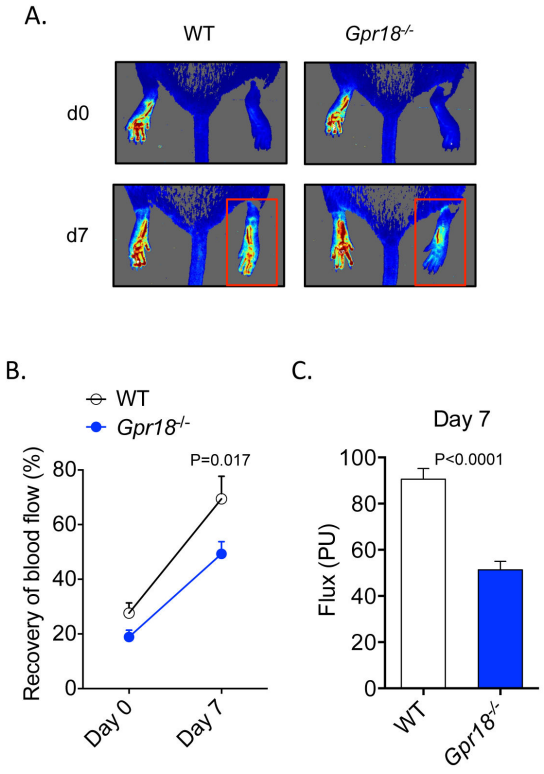

Figure 6. Deficiency of RvD2 receptor, *Gpr18*, impairs perfusion recovery during HLI

(A) Representative laser speckle perfusion imaging in WT and *Gpr18*-KO mice undergoing HLI (d0: day 0; d7: day 7). The red box indicates the ischemic limb. (B) Quantification of limb perfusion in WT and *Gpr18*-KO mice undergoing HLI (% perfusion relative to the non-ischemic limb). (C) Absolute flux (PU: perfusion units) in the ischemic limbs of WT and *Gpr18*-KO mice at day 7. Data are mean ± SEM; n=5-7/group. Statistical comparisons were made using two-way ANOVA, followed by Sidak's multiple comparisons post-tests (B) or an unpaired two-tailed Student's *t* test (C).

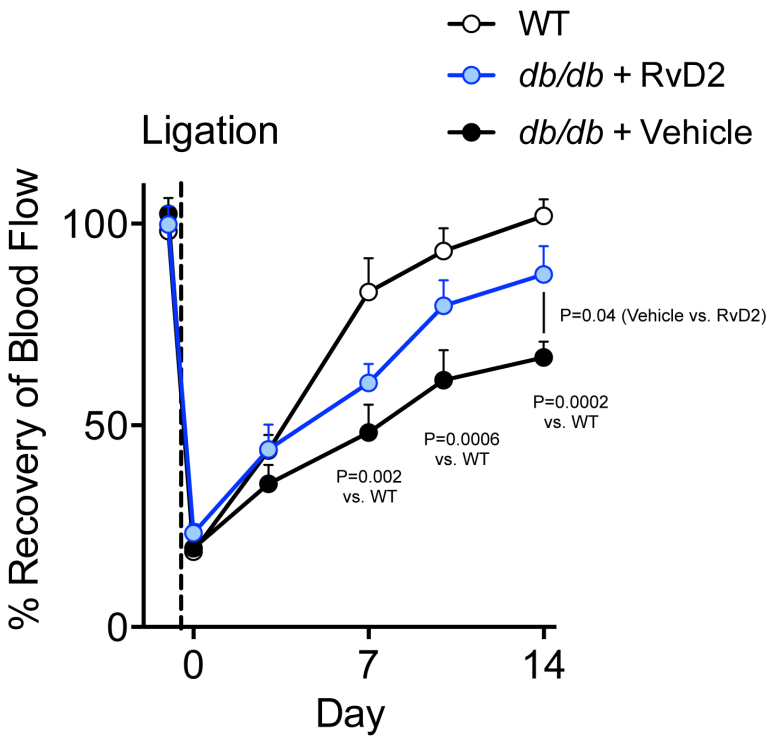

Figure 7. RvD2 rescues defective revascularization in diabetic mice

Quantification of limb perfusion in WT or leptin receptor-deficient (*db/db*) mice undergoing HLI and treated with vehicle or RvD2 for 14 days. Results are presented as % perfusion of the ischemic limb relative to the non-ischemic limb. Data are mean ± SEM; n=3-5/group. Statistical comparisons were made using two-way ANOVA, followed by Sidak's multiple comparisons post-tests, with P-values for specific comparisons indicated.